Extreme Mechanics Letters 38 (2020) 100750

Contents lists available at ScienceDirect

Extreme Mechanics Letters

journal homepage: www.elsevier.com/locate/eml

Buckling-driven periodic wrinkle patterns in a film-lattice structure

Guangzhi Zeng, Tianyu Zhao, Jianlong Chen, Dong Yan, Kai Zhang *

School of Aerospace Engineering, Beijing Institute of Technology, Beijing, 100081, China

A R T I C L E I N F O

Article history:
Received 23 January 2020
Received in revised form 1 April 2020
Accepted 24 April 2020
Available online 28 April 2020

Keywords:
Thin film
Wrinkle
Film-lattice structure
Buckling

A B S T R A C T

Film structures have been widely used in flexible electronics, material science, metrology, biomedical engineering and aerospace engineering. When a thin film is loaded with compressive stresses, buckling accompanied by wrinkles is likely to occur under constrained boundaries. Many previous studies have focused on the wrinkling mechanism of a free-standing film or a film–substrate structure, in which compressive stresses in the film are caused by the mismatch between the film and the imposed constrains from its boundaries or the substrate. Instead of using the homogeneous substrate, here we propose a film-lattice structure consisting of a thin film bonded to a bottom-supported lattice. By controlling the buckling of the lattice structure, a distribution of compressive loads can be applied to the film, finally resulting in the generation of periodic wrinkles. Physical mechanism on the buckling-driven wrinkle pattern is investigated with the increasing loading. Dimensionless parameters and their effect on governing the wrinkling mode are also analyzed numerically. The exploration on features of the wrinkles on the film shows that the wrinkle pattern can be controlled by designing the lattice substrate. Our works could help understand the wrinkling caused by the buckling of a complex substrate and guide the harnessing of wrinkles in the design of new materials and structures.

1. Introduction

Thin films are ubiquitous in nature, such as the surface of lotus leaves, human skin, and small intestine mucosa [1,2]. Since thin film structures have the characteristics of light weight, small folding volume and flexible deployment, they are advantaged for applications in flexible electronics, material science, biomedical engineering and aerospace engineering [3–5]. Owning to their negligible bending stiffness, thin films are prone to wrinkle when undergoing compressive stresses with appropriate constrains, further reducing strain energy by morphing from a compression state to a bending state [6,7]. On one hand, wrinkles will change mechanical performance of the film structure [5,8]. On the other hand, wrinkles can be harnessed to increase the ductility of the electronic devices and measure mechanical properties of some micro/nano materials [9,10]. Early work on wrinkling can be traced back to 1929 when Wagner studied the wrinkles on metal sheets [11–13]. Then, a body of theoretical, numerical and experimental studies were performed to study the wrinkling morphology of thin films under various loading conditions [14–17]. Later, with the increasing demand for controlling the surface pattern of thin films, interests in controlling the characteristics of wrinkle patterns, including wavelength, amplitude and their evolution with loadings, have received much attention in fundamental research and in practical engineering. The wrinkling of film–substrate structures was studied and the wrinkle morphology was controlled by changing the way of the substrate shrinkage of or engraving micro-patterns in the substrate [18–22]. In addition, the stress distribution in a film was also changed to suppress wrinkles or generate different wrinkle patterns by perforating the film [23,24]. In previous studies, the structure of a thin film bonded to a homogeneous substrate is widely used. When the structure is deformed under an external stimulus, the mismatched deformation between the film and the substrate will transform the stimulus into uniform surface traction distributed at their interface. The tunability on winkling pattern of the film is limited and novel mechanism on the controllable winkling pattern is required. Instead of using a homogeneous substrate, by designing microstructure of the substrate, complex loads can be generated on the film and further utilized to form desired wrinkle patterns. So far, the study on the wrinkling of a thin film bonded to a substrate with microstructures is little reported.

Here we propose a film-lattice structure consisting of a thin film bonded to a bottom-supported lattice and a physical mechanism on the buckling-driven wrinkle pattern is investigated with the increasing loading. When the film-lattice structure expands under an external stimulus, the film can form complex periodic wrinkle patterns. Compared with a homogeneous substrate, the lattice generates periodic sinusoidal loads instead of uniform surface traction on the film. We numerically study the effect of

* Corresponding author.
E-mail address: zhangkai@bit.edu.cn (K. Zhang).

https://doi.org/10.1016/j.eml.2020.100750

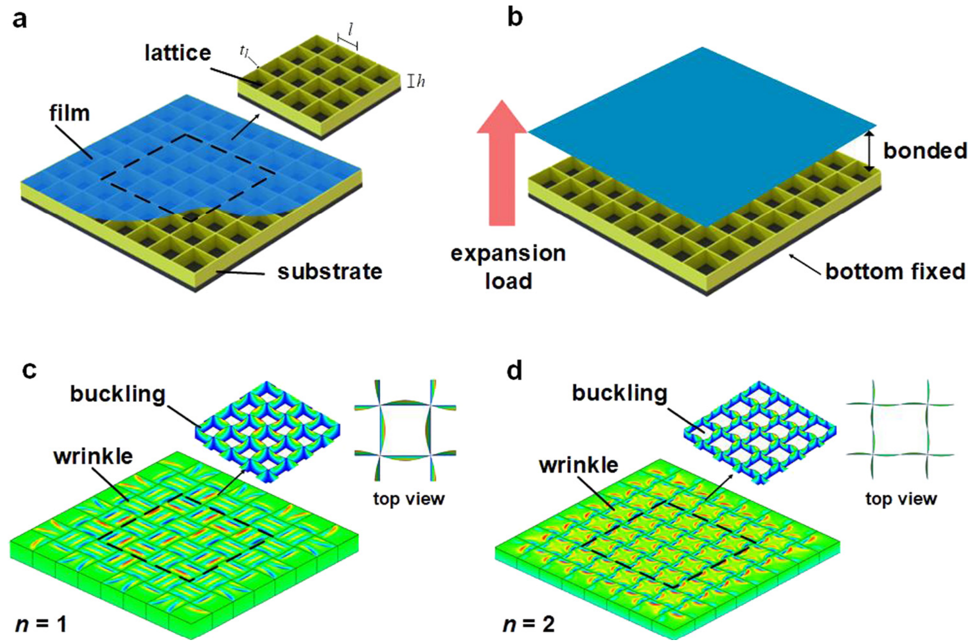

Fig. 1. Schematic of the film-lattice structure and its wrinkle pattern. (a) A film-lattice structure consists of a lattice with crossed slender walls fixed on a rigid ground and a thin film bonded to the top of the lattice. (b) Boundary condition and thermal loading applied on the structure. Wrinkle patterns and the corresponding lattice buckling modes: (c) wave number $n = 1$ and (d) $n = 2$.

material and geometric parameters on the wrinkle pattern and analyze the mechanism of the sinusoidal loads caused by the buckled lattice. At last, we study the evolution of wrinkle pattern and its wavelength with increasing external loads and discuss the underlying mechanism. Our work on the film-lattice structure could be used to guide the suppression of wrinkles or to generate complex wrinkle patterns for the design of new materials and structures.

2. Methods

As shown in Fig. 1a, our film-lattice structure comprises a soft thin film, which is bonded to a bottom-supported lattice substrate. The film in thickness t_f is made of a homogeneous material of Young's modulus E_f and Poisson's ratio ν_f. The crossed thin walls that construct the unit cells of the lattice substrate have dimensions of l in length, h in height, and t_l mm in thickness, with E_l and ν_l as the Young's modulus and Poisson's ratio of the material, respectively.

The deformation of this system is initially driven by the uniform expansion of the lattice, and the corresponding strain is denoted by ε. Constrained by the rigid support at the bottom, the slender walls are compressed in plane. Therefore, when the expansion strain reaches a critical value, buckling of the walls occurs, resulting in wrinkling of the thin film under distributed loads imposed by the buckled lattice.

We perform numerical simulations using the finite element modeling (FEM) package ABAQUS/Standard to study the mechanical response of this film-lattice structure. The film and lattice are modeled by linear elastic materials. The film is bonded to the top of the lattice using tie constraints, where no relative motion is allowed. The bottom of the lattice is fixed on a rigid support (Fig. 1b). Both the lattice and film are meshed using S4R shell elements. To apply an increasing uniform expansion strain to the lattice, we impose different temperature increments in the lattice whose coefficient of thermal expansion is $\alpha = 1e^{-4}/°\mathrm{C}$ and the steady state of the film-lattice structure is considered. The number of elements in each wall and film is 125 and 625, respectively. A mesh sensitivity study has been performed to ensure that the mesh is sufficiently fine. Buckling modes of the lattice are extracted through eigenvalue buckling analysis. To trigger the buckling of the structure in geometrically nonlinear analyses, the first four buckling modes are then imposed into the model as initial geometric imperfections, whose amplitudes are $1\%t_f$, $0.25\%t_f$, $0.063\%t_f$, and $0.016\%t_f$, respectively. An artificial damping is adopted to facilitate the convergence of solutions by setting a stability factor of 2×10^{-8}. Through FEM, we can obtain the deformation of the film-lattice structure in pre-buckling and post-buckling.

3. Results

As shown in Fig. 1c, a film-lattice structure containing 8×8 unit cells is analyzed by FEM. We take the dimensionless material properties and geometric parameters of the structure as $E_l/E_f = 300$, $\nu_f = 0.3$, $\nu_l = 0.3$, and $t_f/l = 0.005$, $h/l = 0.6$, $t_l/l = 0.04$, respectively. Expansion strain ε is imposed in the bottom-supported lattice by raising the temperature, which results in buckling of the walls of the lattice at a critical point. Then, the buckled lattice drives the film to wrinkle, exhibiting a periodic wrinkle pattern, as shown in Fig. 1c. The wrinkles are parallel to each other in the unit cell, while orthogonal in two neighboring unit cells. In comparison, as the aspect ratio of the wall decreases, i.e., $h/l = 0.4$, a different wrinkle pattern with chiral features is observed, as shown in Fig. 1d. The wall of the lattice undergoes a second order buckling mode, where we can find two half waves on each slender wall. Since the second order buckling mode breaks the symmetry of unit cells, the film mainly near the edges of the wall shows chiral wrinkle pattern. Comparing the two representative cases, we find that the buckling mode of the lattice plays an important role in the morphology of wrinkles. The restriction from the fixed boundary at the bottom of the lattice becomes stronger as the aspect ratio of the wall decreases. As a result, the wall buckles in a higher mode. The change of buckling mode of the lattice produces a qualitatively different wrinkle pattern in the film. Different with the previous studies on the wrinkling of film–substrate structures, the winkles here are induced by the buckling of the lattice substrate. We provide

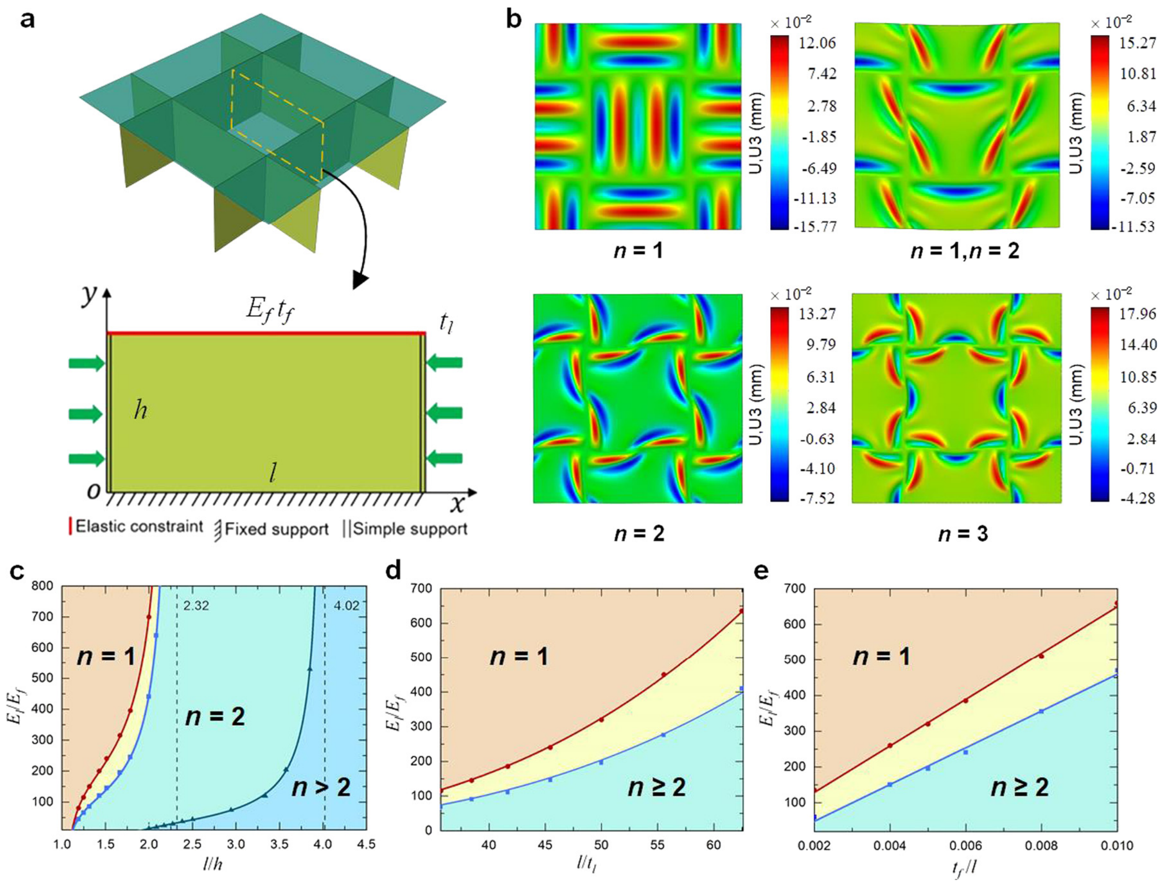

Fig. 2. Wrinkling modes and phase diagrams of film-lattice structures with different material and geometric parameters. (a) Periodic model of the film-lattice structure and equivalent model of the walls in the lattice. (b) Wrinkle patterns of $n = 1$, $n = 1$ and $n = 2$, $n = 2$, $n = 3$. U3 is the out-of-plane displacement of the thin film. (c–e) Phase diagrams of wrinkling modes in the parameter space of (c) E_l/E_f versus l/h, (d) E_l/E_f versus l/t_l, and (e) E_l/E_f versus t_f/l. The yellow region represents the phase of the mixed mode of $n = 1$ and $n = 2$. . (For interpretation of the references to color in this figure legend, the reader is referred to the web version of this article.)

a method to generate various wrinkle patterns in a thin film by controlling the buckling mode of its lattice substrate.

Since the wrinkles in the film exhibit a periodic pattern, we simplify our model to a 2×2 unit cell with periodic boundary conditions imposed on each side (Fig. 2a). For the film-lattice structure, four dimensionless parameters E_l/E_f, t_f/l, t_l/l, and h/l are considered to investigate their effects on the pattern of wrinkles, while the Poisson's ratios of both the film ν_f and lattice ν_l are fixed at 0.3. We analyze the wrinkling mode by FEM simulations and find that different types of wrinkling mode can be distinguished by the number of half waves n in the buckled walls (Fig. 2b). U3 represents the out-of-plane displacement. When $n = 1$, the wrinkles in the film are straight as shown in Fig. 2b, which are perpendicular in two neighboring unit cells. For the mode $n = 2$, chiral wrinkles appear mainly near the edge of the unit cell. A higher order mode ($n = 3$) and a mixed mode ($n = 1$ and $n = 2$) are also observed. In the mixed mode, the number of half waves in the lateral direction of wall is 2, while in the longitudinal wall is 1, resulting in the lateral wrinkle period of $2l$ and longitudinal wrinkle period of l. On the other hand, in wrinkling mode $n = 3$, all the walls in the unit cell exhibit third order buckling mode, resulting in wrinkles on the film with three half waves. The wrinkle in $n = 3$ has the same period l as mode $n = 1$, but shows chirality in the opposite direction between two neighboring unit cells compared with the wrinkle mode of $n = 2$.

Scaling law is a common method to investigate the relationship between the wrinkle pattern and material and geometric parameters. By fitting the data of critical points when structure buckling, the power relationship between the wavelength and amplitude of the wrinkles and the structural parameters can be revealed [7,10,20,24]. We present phase diagrams (Fig. 2c–e) to visualize the relationship between the dimensionless parameters and the wrinkling modes. We first vary l/h in the range from 1 to 4.5 and corresponding ratios of E_l/E_f in the range from 1 to 800. The phase diagram of the wrinkling mode related to the E_l/E_f and l/h is shown in Fig. 2c. Points in the phase diagram represent critical parameters when the wrinkling mode changes, which divides the phase diagram to four regions by three fitting curves. The fitting function shows the relationship between these two parameters as $E_l/E_f = [a + b\ (l/h)]/[1 + c\ (l/h) + d\ (l/h)^2]$. With the increasing E_l/E_f, the phase boundaries get close to two asymptotes $l/h = 2.32$ and $l/h = 4.02$, which are given by the buckling of the lattice without the film bonded on [25]. It means that as the film becomes compliant, the deformation of the film has little effect on the lattice, thus, the buckling mode of the structure will degenerate into a single lattice without the film. The phase diagram of wrinkling mode related to E_l/E_f and l/t_l is shown in Fig. 2d. We select different values of l/t_l ranging from 35 to 65.14 and values of E_l/E_f ranging from 68 to 635. The fitting function shows a cubic relationship $E_l/E_f \propto (l/t_l)^3$ between these two parameters. As l/t_l increases with fixed E_l/E_f, the wall becomes slenderer, resulting in a higher order buckling mode and wrinkling mode. Fig. 2e shows the change of wrinkling mode when t_f/l and E_l/E_f are varied. The E_l/E_f changes with t_f/l linearly. As t_f/l increases, the film imposes a strong constraint on buckling of the lattice. Therefore, the lattice exhibits a higher order buckling mode.

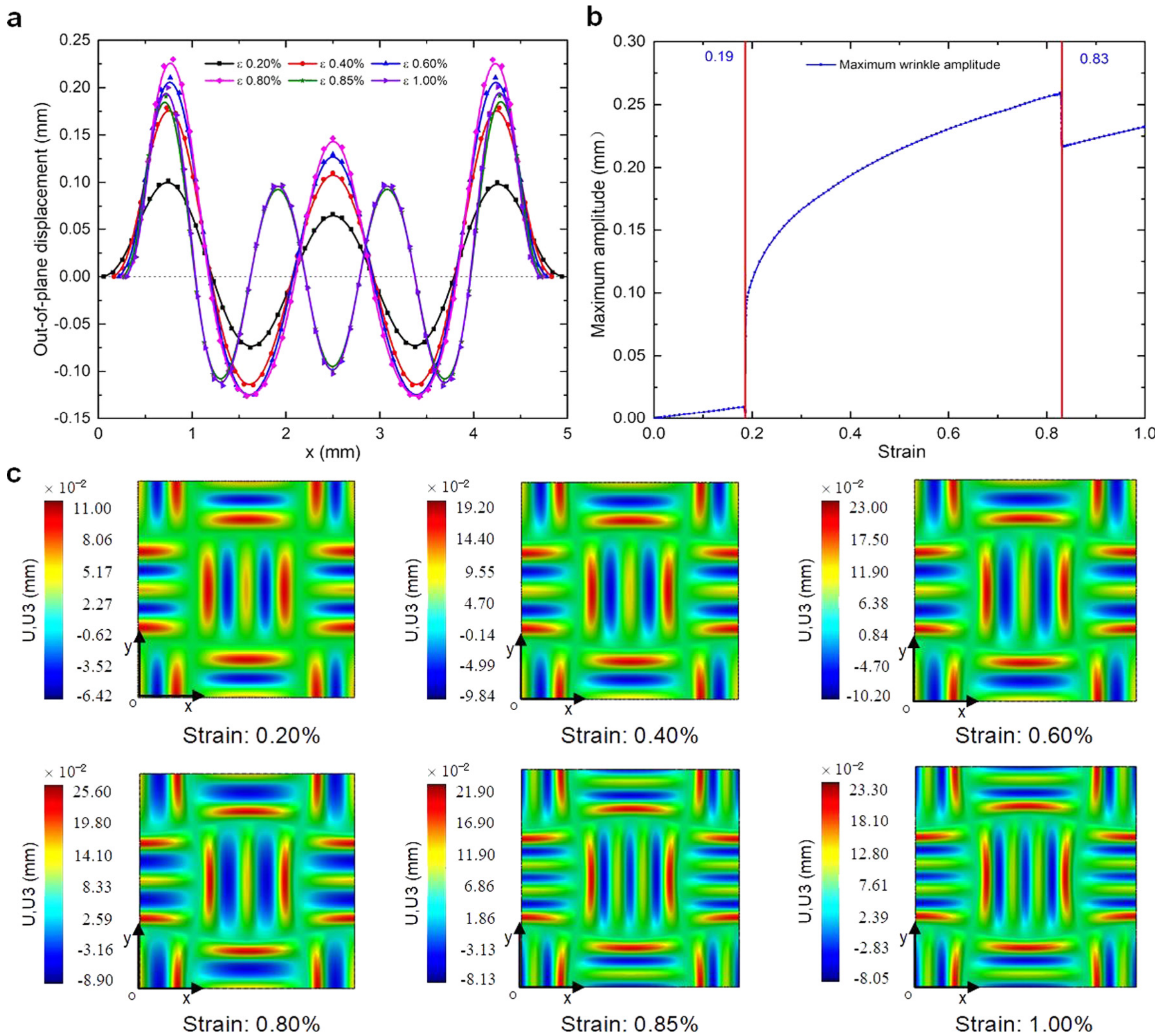

Fig. 3. Evolution of wrinkle pattern of the film-lattice structure under different strains. (a) Wrinkle profiles of the film when strain increases from 0.20% to 1.00%. (b) Wrinkle amplitude as a function of strain. (c) Wrinkle morphologies at different strain levels. U3 is the out-of-plane displacement of the film.

In conclusion, material and geometric parameters are divided into two groups. One is parameter that only related to the geometry of lattice, like l/h, l/t_l. These parameters influence the buckling mode of lattice. The other is the parameters that represent the interaction between film and the lattice, like E_l/E_f and t_f/l. As the E_f or t_f increases, which means stronger interaction are generated on the lattice, the lattice will be buckling at a higher order. But if the film is too compliant to constrain the lattice, the lattice tends to undergo a lower order buckling. Compared with the lattice without a film, the buckling mode of our film-lattice structure is not only related to the aspect ratio of lattice and the length of unit cell, but also to the ratio of Young's moduli between the film and lattice. When the geometry and material of the lattice are fixed, the buckling mode of the structure can still be changed by selecting the modulus of the film. According to the phase diagram, different wrinkling modes can be generated by adjusting the explored parameters.

After the wrinkles are triggered in the film, we gradually increase the load and extract its corresponding wrinkle pattern in the simulation, in order to observe the growth of wrinkles. Here, we focus on the mode $n = 1$ which has a regular wrinkle pattern. The evolution of the film profile along the centerline perpendicular to the wrinkles and the maximum amplitudes with increasing strain are shown in Fig. 3a and b, respectively. Wrinkle patterns at 6 different strain levels are shown in Fig. 3c in details. From Fig. 3, as the strain increases from 0.2% to 0.8%, the wrinkle amplitude increases. However, when the strain further increases to 0.85%, the wave number of the wrinkle pattern jumps from 5 to 7 and the wrinkle amplitude abruptly decreases. Instead of increasing the amplitude of the existed wrinkles, more winkles can be triggered in the film as a response to the increasing strain.

Since the lattice sinusoidal loads are imposed on the film when the film-lattice structure buckles, we remove the lattice and apply sinusoidal displacements directly on the boundaries of the film. Compressive displacements in a sinusoidal distribution with a period of 10 mm are applied to the upper and lower ends of the film. The displacement is maximum at the middle point of the side and 0 at the corners. Meanwhile, the left and right sides are tensioned with the same amplitude and distribution of displacements. The nominal strain in terms of the maximum displacement applied on the sides represents the loading level. The results of wrinkle pattern and its profile along the center line of film perpendicular to the wrinkles are shown in Fig. 4a and b. As shown in Fig. 4a, when the strain increases to 10%, the wrinkle pattern has 9 half waves with the maximum amplitude close to the upper and lower ends of film. From Fig. 4b, the wrinkle amplitude increases with strain until it suddenly drops at $\varepsilon = 8\%$ when new wrinkles form.

To compare with the wrinkle pattern of the film under biaxial loading, we remove the sinusoidal compressive displacements on the upper and lower ends of the film and impose

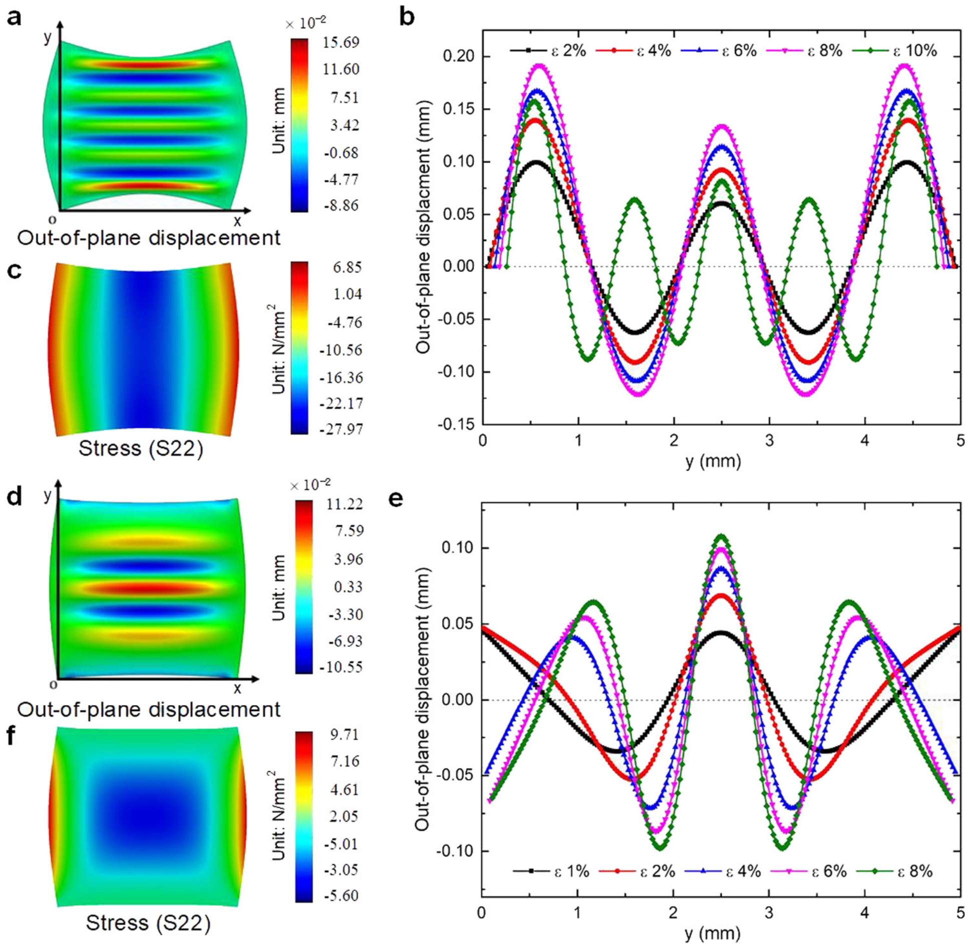

Fig. 4. Wrinkle pattern of a free-standing square film under two types of loading conditions. A square film with sinusoidal displacements imposed at some edges of the film. Wrinkle pattern of the film (a) stretched in the *x* direction and compressed in the *y* direction, and (d) stretched in the *x* direction and free in the *y* direction. (b) and (e) show the wrinkle profiles at different strain levels along the center line of the film corresponding to the two types of loading conditions imposed in (a) and (d), respectively. The distribution of stresses in the *y* direction before the wrinkles formed are presented in (c) and (f), under the two types of loading conditions imposed in (a) and (d), respectively.

free boundary condition. According to the results in Fig. 4d and e, the wrinkles are centralized in the film and the wrinkle of maximum amplitude appears at the center. Moreover, the wavelength decreases and the amplitude monotonically increases with stretching. We further show the compressive stresses before the wrinkles formed in the *y* direction under the two different loading conditions in Fig. 4c and f. When compressive displacements are applied to the upper and lower ends, the compressive stress decreases from the middle to the left and right sides while remains almost constant in the *y* direction. However, the stress reaches a maximum at the center and drops toward boundaries when the upper and lower ends are free. The stress field in the *y* direction is consistent with the distribution of wrinkles. In addition, the compressive loads on the upper and lower end lead to an increase in wrinkle amplitude, especially near the loading area. Since the out-of-plane displacement is fixed when applying the compressive load, the amplitude at the upper and lower end of film is consistently zero, resulting in a gradient rather than continuous change in the wrinkle wavelength. By comparison, we find that biaxial sinusoidal loading is more similar to the driving force for wrinkling.

The relationship between the wavelength of wrinkles and the size of film is further investigated. The side length of the film is varied from 5 to 200 mm and the same biaxial sinusoidal displacements are applied on the film. From the results shown in Fig. 5a, wrinkle wavelength increases with film size under all 4 strain levels at $\varepsilon = \{2.5\%, 5.0\%, 7.5\%, 10.0\%\}$. In addition, the number of wrinkles as a function of strain for the film size of 5 mm and 100 mm are shown in Fig. 5b and c. At the film size of 5 mm, the wrinkle number changes from 3 to 5 at $\varepsilon = 0.1\%$, and 5 to 9 at the at $\varepsilon = 10\%$. In comparison, when film size increases to 100 mm, the wrinkle number changes from 4 to 30 through 12 discrete stages when strain gradually increases. The film size does not affect the jumping phenomenon of number of wrinkles. But as the film size increases, the jumping phenomenon is more frequent. Notably, the jumping phenomenon of wrinkle number also exists during unloading but follows a different path, as shown in Fig. 5c.

4. Conclusions

In summary, we propose a film-lattice structure comprising a soft thin film bonded to a lattice structure with crossed slender walls. Under isotropic expansion, periodic wrinkle patterns in the film generated by buckling of the lattice structure are found. The mechanism on the wrinkling is the biaxial sinusoidal loading caused by the buckled lattice. Different modes of wrinkle patterns can be tailored by changing the material properties and dimensions of the lattice according to the phase diagrams. The wrinkle wavelength, amplitude and their evolution with the increasing strain are analyzed and a jumping phenomenon of wrinkle number is revealed. The mechanism of film wrinkling

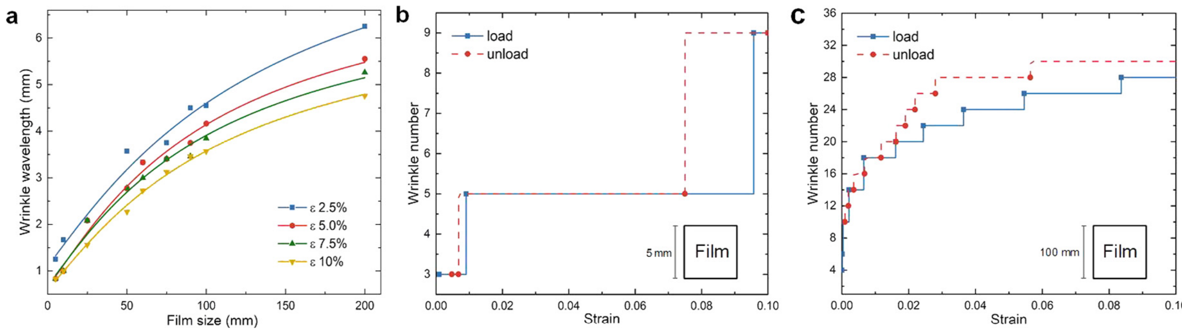

Fig. 5. Effect of the film size on the wrinkle morphology. (a) Wrinkle wavelength versus film size at different strain levels. The number of wrinkles as a function of strain for a film of side length (b) 5 mm or (c) 100 mm.

driven by the buckling of a lattice substrate discussed in this work could help understand the wrinkling of thin films under complex constrains and guide the harnessing of wrinkles in the design of new materials and structures.

Declaration of competing interest

The authors declare that they have no known competing financial interests or personal relationships that could have appeared to influence the work reported in this paper.

Acknowledgments

This work was supported by National Natural Science Foundation of China (Grant No. 11672037, No. 11991031).

K. Z. conceived the project. G.Z, T.Z and J.C. performed numerical simulation. G.Z and J.C did the data analysis. K. Z. discussed the results assisted with G. Z and D.Y. All authors contributed to the writing of the paper.

References

[1] A. Nakajima, K. Hashimoto, T. Watanabe, Recent studies on super-hydrophobic films, in: W.J. Blau, P. Lianos, U. Schubert (Eds.), Molecular Materials and Functional Polymers, Springer, Vienna, 2001, pp. 31–41.
[2] T. Savin, N.A. Kurpios, A.E. Shyer, P. Florescu, H. Liang, L. Mahadevan, C.J. Tabin, On the growth and form of the gut, Nature 476 (2011) 57–62.
[3] J. Kim, J. Yoon, R.C. Hayward, Dynamic display of biomolecular patterns through an elastic creasing instability of stimuli-responsive hydrogels, Nature Mater. 9 (2010) 159–164.
[4] J.A. Rogers, T. Someya, Y. Huang, Materials and mechanics for stretchable electronics, Science 327 (2010) 1603–1607.
[5] W. Wong, S. Pellegrino, Wrinkled membranes I: experiments, J. Mech. Mater. Struct. 1 (2006) 3–25.
[6] B. Budiansky, Theory of buckling and post-buckling behavior of elastic structures, in: C.-S. Yih (Ed.), Advances in Applied Mechanics, Elsevier, 1974, pp. 1–65.
[7] E. Cerda, L. Mahadevan, Geometry and physics of wrinkling, Phys. Rev. Lett. 90 (2003) 074302.
[8] J.R. Blandino, J.D. Johnston, U.K. Dharamsi, Corner wrinkling of a square membrane due to symmetric mechanical loads, J. Spacecr. Rockets 39 (2002) 717–724.
[9] D.-Y. Khang, H. Jiang, Y. Huang, J.A. Rogers, A stretchable form of single-crystal silicon for high-performance electronics on rubber substrates, Science 311 (2006) 208–212.
[10] J. Huang, M. Juszkiewicz, W.H. de Jeu, E. Cerda, T. Emrick, N. Menon, T.P. Russell, Capillary wrinkling of floating thin polymer films, Science 317 (2007) 650–653.
[11] H. Wagner, Flat Sheet Metal Girders with Very Thin Metal Web. Part I: General Theories and Assumptions, NACA Technical Memorandum. 604, 1931.
[12] H. Wagner, Flat Sheet Metal Girders with Very Thin Metal Web. Part II: Sheet Metal Girders with Spars Resistant To Bending - Oblique Uprights - Stiffness, NACA Technical Memorandum. 605, 1931.
[13] H. Wagner, Flat Sheet Metal Girders with Very Thin Metal Web. Part I: Sheet Metal Girders with Spars Resistant To Bending - the Stress in Uprights - Diagonal Tension Fields, NACA Technical Memorandum. 606, 1931.
[14] E. Cerda, K. Ravi-Chandar, L. Mahadevan, Wrinkling of an elastic sheet under tension, Nature 419 (2002) 579–580.
[15] N. Friedl, F.G. Rammerstorfer, F.D. Fischer, Buckling of stretched strips, Comput. Struct. 78 (2000) 185–190.
[16] V. Nayyar, K. Ravi-Chandar, R. Huang, Stretch-induced stress patterns and wrinkles in hyperelastic thin sheets, Int. J. Solids Struct. 48 (2011) 3471–3483.
[17] V. Nayyar, K. Ravi-Chandar, R. Huang, Stretch-induced wrinkling of polyethylene thin sheets: Experiments and modeling, Int. J. Solids Struct. 51 (2014) 1847–1858.
[18] P.J. Yoo, K.Y. Suh, S.Y. Park, H.H. Lee, Physical self-assembly of microstructures by anisotropic buckling, Adv. Mater. 14 (2002) 1383–1387.
[19] W.T.S. Huck, N. Bowden, P. Onck, T. Pardoen, J.W. Hutchinson, G.M. Whitesides, Ordering of spontaneously formed buckles on planar surfaces, Langmuir 16 (2000) 3497–3501.
[20] Z.Y. Huang, W. Hong, Z. Suo, Nonlinear analyses of wrinkles in a film bonded to a compliant substrate, J. Mech. Phys. Solids 53 (2005) 2101–2118.
[21] N. Bowden, S. Brittain, A.G. Evans, J.W. Hutchinson, G.M. Whitesides, Spontaneous formation of ordered structures in thin films of metals supported on an elastomeric polymer, Nature 393 (1998) 146–149.
[22] Z. Huang, W. Hong, Z. Suo, Evolution of wrinkles in hard films on soft substrates, Phys. Rev. E. 70 (2004) 030601.
[23] D. Yan, K. Zhang, F. Peng, G. Hu, Tailoring the wrinkle pattern of a microstructured membrane, Appl. Phys. Lett. 105 (2014) 071905.
[24] D. Yan, K. Zhang, G. Hu, Wrinkling of structured thin films via contrasted materials, Soft Matter 12 (2016) 3937–3942.
[25] S.H. Kang, S. Shan, W.L. Noorduin, M. Khan, J. Aizenberg, K. Bertoldi, Buckling-induced reversible symmetry breaking and amplification of chirality using supported cellular structures, Adv. Mater. 25 (2013) 3380–3385.